Volume 1 | Number 1 | Jan 2013 | Pages 1–100

Catalysis
Science &
Technology

www.rsc.org/catalysis

ROYAL SOCIETY
OF CHEMISTRY

This is an *Accepted Manuscript*, which has been through the Royal Society of Chemistry peer review process and has been accepted for publication.

Accepted Manuscripts are published online shortly after acceptance, before technical editing, formatting and proof reading. Using this free service, authors can make their results available to the community, in citable form, before we publish the edited article. We will replace this *Accepted Manuscript* with the edited and formatted *Advance Article* as soon as it is available.

You can find more information about *Accepted Manuscripts* in the **Information for Authors**.

Please note that technical editing may introduce minor changes to the text and/or graphics, which may alter content. The journal's standard **Terms & Conditions** and the **Ethical guidelines** still apply. In no event shall the Royal Society of Chemistry be held responsible for any errors or omissions in this *Accepted Manuscript* or any consequences arising from the use of any information it contains.

ROYAL SOCIETY
OF CHEMISTRY

www.rsc.org/catalysis

Amount of Tungsten Dopant Influencing the Photocatalytic Water Oxidation Activity of LaTiO$_2$N Crystals Grown Directly by an NH$_3$-Assisted Flux Method

Kenta Kawashima[1], Mirabbos Hojamberdiev[1], Hajime Wagata[1], Masanobu Nakayama[2],

Kunio Yubuta[3], Shuji Oishi[1], Kazunari Domen[4], and Katsuya Teshima[1,5],*

[1]Department of Environmental Science and Technology, Faculty of Engineering, Shinshu University, 4-17-1 Wakasato, Nagano 380-8553, Japan

[2]Department of Materials Science and Engineering, Nagoya Institute of Technology, Gokiso, Showa, Nagoya, Aichi 466-8555, Japan

[3]Institute for Materials Research, Tohoku University, 2-1-1 Katahira, Aoba-ku, Sendai 980-8577, Japan

[4]Department of Chemical System Engineering, School of Engineering, The University of Tokyo, 7-3-1 Hongo, Bunkyo-ku, Tokyo 113-8656, Japan

[5]Center for Energy and Environmental Science, Shinshu University, 4-17-1 Wakasato, Nagano 380-8553, Japan

---

*Corresponding Author

Phone: +81-26-269-5541. Fax: +81-26-269-5550. E-mail: teshima@shinshu-u.ac.jp

Abstract

Solar water splitting technologies for hydrogen generation using visible-light-active (oxy)nitride photocatalysts have been intensively studied to achieve a greater supply of clean and renewable energy. Here, we have investigated the amount of tungsten dopant influencing the photocatalytic water oxidation activity of $LaTiO_2N$ (LTON) crystals grown directly by an NH_3-assisted KCl flux method in the absence of cocatalyst. With the maximum amount of tungsten dopant ($x = 0.10$), $LaWO_{0.6}N_{2.4}$ was formed as a minor phase to the W-doped $LaTiO_2N$ phase (W-LTON). The optimum W-doped $LaTiO_2N$ crystals were grown with the tungsten amount of $x = 0.05$, showing the nearly three-fold higher O_2 evolution rate (51 $\mu mol \cdot h^{-1}$) compared to pure $LaTiO_2N$ crystals (18 $\mu mol \cdot h^{-1}$). The improvement in O_2 evolution rate of the $LaTiO_2N$ crystals was due presumably to the improved conductivity, enhanced light absorption, and efficient charge separation stemmed from tungsten doping. According to the first-principles density function theory (DFT) calculations, although no significant change in band gap by tungsten doping was observed, a slight broadening of valence and conduction bands was noted in W-LTON which may improve the electron/hole conductivity due to reducing the effective mass of electron. Also, tungsten doping was beneficial in creating the effective defects and in enhancing the photocatalytic water oxidation activity of the $LaTiO_2N$ crystals.

Keywords: LaTiO$_2$N; Water oxidation; Flux Growth; Tungsten doping; Transition Metal; Oxynitride

Introduction

Photocatalytic overall water splitting to generate hydrogen and oxygen over (oxy)nitride photocatalysts using solar energy has been studied as one of the potential approaches to fulfill a growing demand for clean and renewable energy as well as to solve serious environmental issues.[1,2] Having a band gap of about 2.1 eV ($\lambda = ca.$ 600 nm), lanthanum titanium oxynitride (LaTiO$_2$N) is a member of the visible-light-active (oxy)nitride photocatalysts family and has shown a good photocatalytic activity for hydrogen and oxygen generation from water splitting in the presence of suitable sacrificial reagents under visible light because of its appropriate band positions.[3,4] The achievable theoretical potential of a photocatalyst with a visible light absorption edge of 600 nm is 16.2% solar-energy-conversion efficiency (assuming an overall water splitting quantum yield of unity).[5] Recent reports have demonstrated that the solid solution ((SrTiO$_3$)$_{1−x}$·(LaTiO$_2$N)$_x$),[6] doping cations A or B site in ABO$_x$N$_y$ ((La,Ca)Ti(O,N)$_3$ and LaTi$_{1−x}$M$_x$(O,N)$_{3\pm\delta}$ (x = 0 and 0.1, M = Nb^{5+}, W^{6+})),[7,8] and loading various cocatalysts (IrO$_x$, CoO$_x$, Co$_3$O$_4$)[9-11] were beneficial for the improvement of photocatalytic performance of LaTiO$_2$N. However, various charge carrier recombination paths lead to lower water splitting activity of LaTiO$_2$N.

Flux growth method has been demonstrated as one of the straightforward techniques to improve the photocatalytic activity of inorganic crystals by reducing the density of defects, which act as recombination centers for photogenerated electrons and holes in the crystals.[12,13] For instance, the $LaTiO_2N$ crystals fabricated by nitridation of the $La_2Ti_2O_7$ precursor under an NH_3 flow with and without flux exhibited higher photocatalytic activity for water oxidation.[10,14] Recently, we have also grown the $LaTiO_2N$ crystals with less defect density and high crystallinity by a direct NH_3-assisted flux method using the KCl flux, and higher photocatalytic activity for water oxidation was achieved.[15] Furthermore, doping the semiconductor-based photocatalysts with transition-metal cations having partly filled d orbitals has also improved the photocatalytic activity through the effect that the transition-metal cations can behave as a center for absorption of visible light because of the formed donor or acceptor level in the forbidden band of the host material.[16,17] Particularly, the tungsten doping significantly improved the electron lifetime and enhanced the photocatalytic activity of Ta_3N_5 and $BaTaO_2N$ due to the faster interface charge transfer and the suppressed recombination and photocorrosion of the W-doped Ta_3N_5 photoelectrode[18] and the pronounced upward band-bending character of the W-doped $BaTaO_2N$, allowing an easy migration of holes to the surface.[19] In this work, we report on the direct growth of the W-doped $LaTiO_2N$ crystals by an NH_3-assisted flux method using the KCl flux, and the photocatalytic activity for water oxidation of pure and W-doped $LaTiO_2N$ crystals was comparatively studied with respect to the doping amount of tungsten.

Experimental

An NH_3-assisted flux growth of the W-doped $LaTiO_2N$ ($LaTi_{1-x}W_x(O,N)_3$) crystals was performed using reagent-grade La_2O_3, TiO_2, $Na_2WO_4 \cdot 2H_2O$, and KCl (> 98%, Wako Pure Chemical Industries, Ltd.). The well-homogenized mixture of La_2O_3, TiO_2, and $Na_2WO_4 \cdot 2H_2O$ in stoichiometric ratio was used as a solute, and KCl was employed as a flux. The solute (W-doped $La_2Ti_2O_7$) concentration was defined as 5 mol%, and the total mass of a solute-flux mixture was approximately 3.0 g for each run. To study the effect of the amount of tungsten dopant on the crystal growth, phase evolution, and photocatalytic water oxidation activity, x was changed from 0.00 to 0.10 in $LaTi_{1-x}W_x(O,N)_3$. After manual dry mixing for 30 min, each solute-flux mixture was placed in a platinum cell with a capacity of 4.0 cm^3, heated at 950 °C for 10 h at a heating rate of 600 °C·h^{-1} under an NH_3 flow (200 mL·min^{-1}), and cooled naturally. The flux-grown crystals were separated from the remaining flux by washing the final crystal products with warm water and dried at 100 °C for 10 h.

The crystalline phases of the flux-grown crystals were identified by X-ray diffraction (XRD, MiniflexII, Rigaku). The morphology and size of the crystals were observed by field-emission scanning electron microscopy (FE-SEM, JSM-7600F, JEOL). The amount of tungsten dopant (Ti:W ratio) in the flux-grown crystals was analyzed by inductively coupled plasma - optical emission spectrometry (ICP-OES, SPS5510, SII Nanotechnology Inc.). The Brunauer, Emmett, and Teller (BET) specific surface areas (S_{BET}) of the flux-grown crystals were obtained from the N_2

5

adsorption-desorption isotherms at 77 K by using a BELSORP-mini instrument (BEL Japan, Inc.).

The ultraviolet-visible (UV-Vis) diffuse reflectance spectra were recorded on a JASCO V-630

spectrophotometer.

The photocatalytic O_2 evolution experiments were conducted with 100 mg of bare crystals and 200

mg of La_2O_3 (pH buffer) dispersed in 300 mL of 10 mM $AgNO_3$ (> 99%, Wako Pure Chemical

Industries, Ltd.) solution (sacrificial electron scavenger) in a glass cell connected to a

closed-circulation system. A 300W Xe lamp fitted with a cold mirror (CM-1) and a cutoff filter ($\lambda >$

420 nm) was used as a visible light source. The evolved gases were detected by a gas

chromatograph (GC-8A, TCD, Ar gas carrier, Shimadzu).

The structural relaxation for pure $LaTiO_2N$ (LTON), tungsten doped LTON (W-LTON), and

non-nitrided oxide (LTO) was performed by first-principles density function theory (DFT)

calculations with the Vienna Ab Initio Simulation Package[20,21] using the modified

Perdew-Burke-Ernzerhof generalized gradient approximation (PBEsol-GGA)[22,23] and the

projector-augmented wave (PAW) method.[24] A spin polarization calculation was used, a kinetic

cutoff energy was 500 eV, and k-point mesh was set as satisfying a convergence test (< 5

meV/$LaTiO_2N$). The initial configuration of LTON was referred to the previous report of combined

synchrotron and neutron diffraction and DFT study by Yashima et $al.$[25] For the comparison

purpose, we have also investigated the electronic structure of LTO in which all the nitride ions, N^{3-},

in LTON were replaced by oxide ion, O^{2-}, (O_N^{-}), and the total number of electrons in the lattice was

controlled to be $[LaTiO_3]^+$. A jellium background was used to neutralize the lattice with charged

point defects. The exact composition of the calculated cell was $La_4Ti_4O_8N_4$ and $La_4Ti_4O_{12}$ for

LTON and LTO, respectively, and $\sqrt{2} \times 2 \times \sqrt{2}$ against conventional perovskite unit cell was used.

For W-LTON, we expanded the simulation cell to a size of $2 \times 2 \times 2$ conventional perovskite unit

cell to model the point defect of W^{6+} ion at Ti^{4+} site ($W_{Ti}^{\cdot\cdot}$), and two oxide ions were replaced by

nitride ions for charge compensation. The resulting composition of the W-LTON cell was

$La_8WTi_7O_{14}N_{10}$ for present computation. W/Ti or O/N was randomly arranged at each cation or

anion site, and the total electron energy was computed for 8 candidates. The cell with the lowest

total energy was chosen for further electronic structure analysis. Because the band gaps of both

compounds were underestimated, which is typical of the GGA functional,[26] the

Heyd-Scuseria-Ernzerhof (HSE06) hybrid functional was used to estimate the band gaps of LTON,

W-LTON, and LTO. The details are described in Refs. 27, 28. Due to the large computational cost

for HSE06 functional, the relaxed ionic configuration by GGA functional was used in this study.

Results and discussion

Figure 1 shows the XRD patterns of pure and W-doped $LaTiO_2N$ crystals grown by an NH_3-assisted

KCl flux method with different amounts of tungsten dopant ($LaTi_{1-x}W_x(O,N)_3$: $x = 0.00, 0.01, 0.02,$

0.05, and 0.10). The XRD patterns of the crystals grown with the tungsten amounts of $x = 0.00$ -

0.05 were identical to the International Centre for Diffraction Data Powder Diffraction File (ICDD

PDF 48-1230) data for $LaTiO_2N$ with the orthorhombic crystal structure. A further increase in the

amount of tungsten dopant to $x = 0.10$ caused the formation of $LaWO_{0.6}N_{2.4}$ (ICDD PDF 84-1682)

as an impurity phase to $LaTiO_2N$. In accordance with increasing the amount of tungsten dopant

from $x = 0.00$ to $x = 0.05$, the main *112* diffraction peak at 32.08° in the XRD patterns of the

flux-grown crystals shifted slightly to a lower angle due possibly to the presence of the

substitutional tungsten species in the $LaTiO_2N$ crystal lattice. In this case, Ti^{4+} can be replaced with

W^{4+}, W^{5+} or W^{6+} because of similar ionic radius of Ti^{4+} (0.61 Å) with that of W^{4+} (0.66 Å), W^{5+}

(0.62 Å), and W^{6+} (0.60 Å) under such a condition that each coordination number is 6.[29-31] In

previous reports on W-doped and W–N-codoped TiO_2, Ti^{4+} was substituted with W^{6+}; therefore, the

diffraction peaks of the crystals were shifted to a higher angle due to the fact that the ionic radius of

W^{6+} is smaller than that of Ti^{4+}.[32-34] On the contrary, the main *112* diffraction peak shifted slightly

to a lower angle in the present study. The shift of the *112* diffraction peak to a lower angle is

associated with the expansion of the lattice volume caused by the substituted tungsten species (W^{4+}

and W^{5+}) and the mild lattice strain caused by the repulsion between interstitial tungsten dopants.[29]

With the tungsten amount of $x = 0.10$, the main *112* peak shifted slightly to a higher angle with

respect to that of other W-doped $LaTiO_2N$ crystals ($x = 0.01$ - 0.05) due to the reason that all

tungsten source could not be doped in the $LaTiO_2N$ crystal structure because of the separation of the
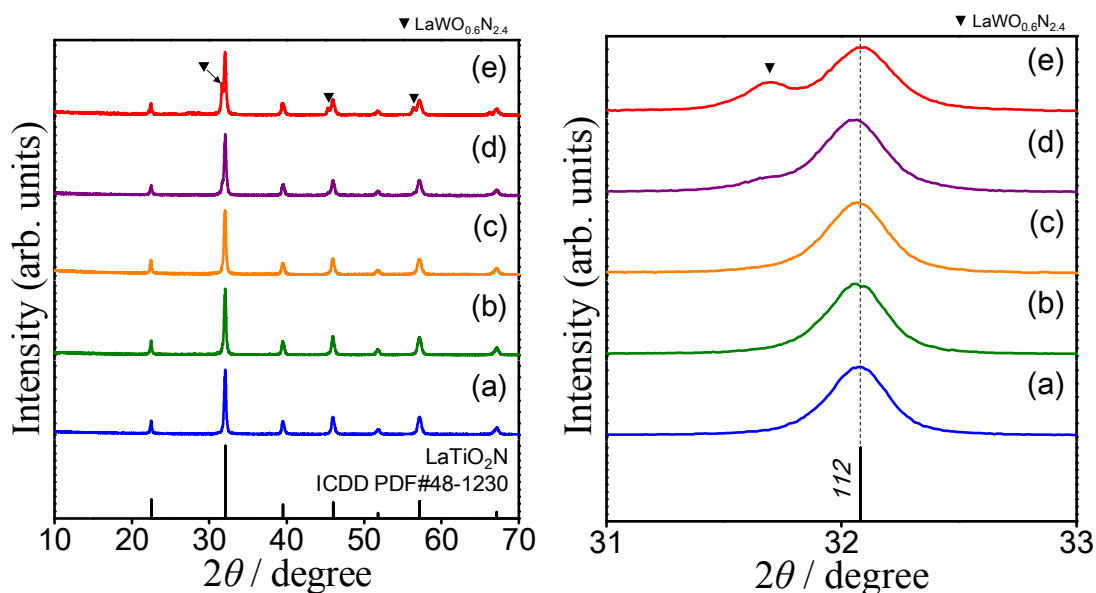
$LaWO_{0.6}N_{2.4}$ crystal phase during the flux growth.

Figure 1. XRD patterns of $LaTi_{1-x}W_x(O,N)_3$: (a) $x = 0.00$, (b) $x = 0.01$, (c) $x = 0.02$, (d) $x = 0.05$, and (e) $x = 0.10$) crystals directly grown by an NH_3-assisted KCl flux method.

Figure 2 shows the SEM images and EDS spectra of pure and W-doped $LaTiO_2N$ crystals grown directly by an NH_3-assisted KCl flux method. As shown in the SEM images, with increasing the amount of tungsten dopant from $x = 0.00$ to $x = 0.05$, the flux-grown crystals with a rounded shape have the average crystal sizes of about 178, 234, 227, and 206 nm, respectively. However, when the amount of tungsten dopant reached $x = 0.10$, the flux-grown crystals possess two different morphologies: small rounded (about 210 nm in size) and large cuboid (about 396 nm in size). According to the EDS results (not shown here), small rounded crystals belong to the W-doped $LaTiO_2N$ phase and large cuboid crystals to the $LaWO_{0.6}N_{2.4}$ phase. Moreover, the amount of incorporated tungsten species in the flux-grown crystals was monotonously increased with increasing the amount of tungsten source in the starting mixture, as judged from the EDS spectra.

9

Also, the exact amount of tungsten species doped in the $LaTi_{1-x}W_x(O,N)_3$ crystals grown with $x =$ 0.01, 0.02, 0.05, and 0.10 was analyzed by ICP-OES and found to be 0.014, 0.021, 0.053 and 0.101, respectively, which are closer to the starting compositions. However, the exact amount of tungsten species in the $LaTi_{1-x}W_x(O,N)_3$ crystals grown with $x = 0.10$ could not be decided due to the presence of two phases ($LaTiO_2N$ and $LaWO_{0.6}N_{2.4}$).

According to our previous report,[15] the small rounded W-doped $LaTiO_2N$ crystals could be grown through the following processes: (i) the formation of the W-doped $La_2Ti_2O_7$ crystals at lower temperatures and shorter times of nitridation due to the lack of atomic nitrogen, (ii) the conversion of the W-doped $La_2Ti_2O_7$ crystals into the W-doped $LaTiO_2N$ crystals under an NH_3 flow with the assistance of the KCl flux, and (iii) the growth of the W-doped $LaTiO_2N$ crystals through the dissolution-precipitation processes and due to the Gibbs-Thomson effect.[35] Meantime, with the maximum amount of tungsten dopant ($x = 0.10$), large cuboid $LaWO_{0.6}N_{2.4}$ crystals with tetragonal symmetry could also be grown along with the W-doped $LaTiO_2N$ crystals because the crystal faces with lower surface energy became prominent.[36,37]
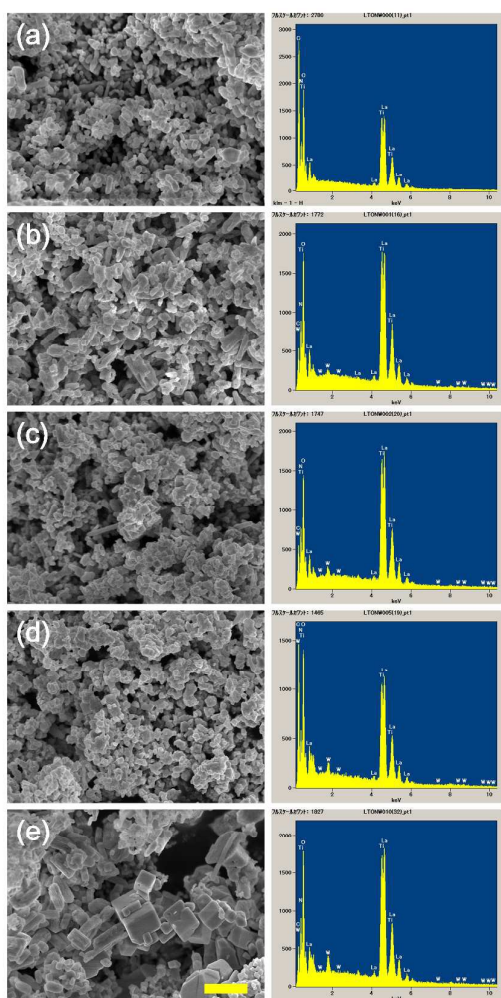
Figure 2. SEM images and EDS spectra of LaTi$_{1-x}$W$_x$(O,N)$_3$: (a) x = 0.00, (b) x = 0.01, (c) x = 0.02,

(d) x = 0.05, and (e) x = 0.10) crystals directly grown by an NH$_3$-assisted KCl flux method. The
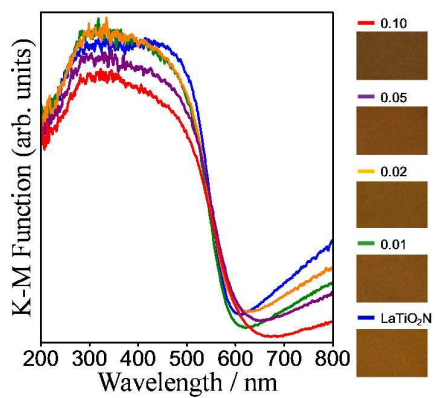
scale bar is 1 μm.

Figure 3. UV-Vis diffuse reflectance spectra of $LaTi_{1-x}W_x(O,N)_3$ (x = 0.00, 0.01, 0.02, 0.05, and 0.10) crystals directly grown by an NH_3-assisted KCl flux method.

Figure 3 shows the UV-Vis diffuse reflectance spectra of pure and W-doped $LaTiO_2N$ crystals grown directly by an NH_3-assisted KCl flux method. The absorption-edge wavelength of pure $LaTiO_2N$ crystals is approximately 589 nm, and the estimated band-gap energy is 2.11 eV. In contrast, the absorption-edge wavelengths of the W-doped $LaTiO_2N$ crystals shifted slightly toward the red end of the spectrum (λ = 589 - 610 nm) with increasing the amount of tungsten dopant, resulting in slightly narrower band-gap energies (E_g = 2.03 - 2.11 eV) compared to that of pure $LaTiO_2N$ crystals. With increasing the amount of tungsten dopant, the color of the flux-grown crystals altered from light brown to dark brown, as shown in Figure 3. In previous reports on W-doped and W–N-codoped TiO_2, the red-shifted absorption-edge wavelength for the tungsten-doped crystals was related to the charge transfer between the valence (N 2p or/and O 2p) to conduction (Ti 3d) bands of TiO_2 and tungsten dopant level.[31-34,38,39] In W–N-codoped TiO_2, the synergistic doping effect of tungsten and nitrogen increased the solubility limits of tungsten and nitrogen.[33] In our case, the tungsten doping made a slight red shift of the absorption-edge wavelength and narrowed the band gap energy of the $LaTiO_2N$ crystals. Presumably, the tungsten doping could promote the inclusion of more interstitial nitrogen in the lattice of the $LaTiO_2N$ crystals compared to pure $LaTiO_2N$ crystals. It is known that the conduction and valence bands of $LaTiO_2N$ are mainly consisted of the orbital of Ti 3d and the hybrid orbital of O 2p and N 2p,

respectively, and the potential of N 2p orbital is higher than that of O 2p orbital by using normal

hydrogen electrode (NHE) as a standard potential.[40] As a result, the top of valence band becomes

higher with increasing the amount of interstitial nitrogen in the W-doped LaTiO$_2$N crystals,

narrowing the band-gap energy of the flux-grown crystals.[41] Therefore, it can be concluded that a

slight shift in the absorption-edge wavelength for the W-doped LaTiO$_2$N crystals was possibly

stemmed from two factors: the charge transfer between the valence band or conduction band and

tungsten dopant level in the W-doped LaTiO$_2$N crystals and the narrowing of the band-gap energy
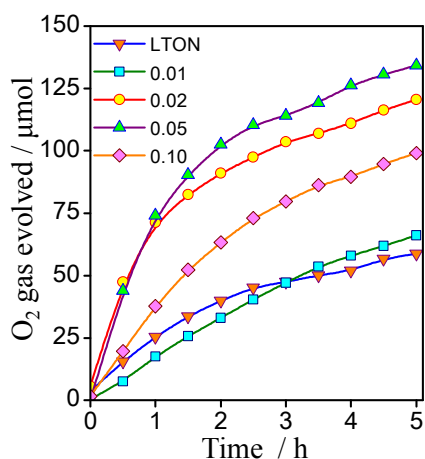
with an increased amount of interstitial nitrogen.

Figure 4. Reaction time courses of photocatalytic O$_2$ evolution of LaTi$_{1-x}$W$_x$(O,N)$_3$ (x = 0.00, 0.01,

0.02, 0.05, and 0.10) crystals directly grown by an NH$_3$-assisted KCl flux method. Photocatalytic

reaction conditions: 100 mg photocatalyst loaded with CoO$_x$ cocatalyst (2 wt% Co); aqueous

solution of AgNO$_3$ (10 mM, 300 mL); 200 mg La$_2$O$_3$ (pH buffer); light source – 300W Xe lamp

fitted with a cold mirror (CM-1) and a cutoff filter (λ > 420 nm); a side-irradiation-type reaction

vessel was used in this study.

Figure 4 shows the reaction time courses of the photocatalytic O_2 evolution over pure and

W-doped $LaTiO_2N$ crystals grown directly by an NH_3-assisted KCl flux method. Within the first 2

h of the photocatalytic O_2 evolution reaction, the maximum O_2 evolution rate (51 $\mu mol \cdot h^{-1}$) was

achieved by the W-doped $LaTiO_2N$ crystals with the tungsten amount of $x = 0.05$ which is nearly

three-fold greater than that of pure $LaTiO_2N$ (18 $\mu mol \cdot h^{-1}$). Probably, this improvement in

photocatalytic O_2 evolution is attributed to the enhanced conductivity of the W-doped $LaTiO_2N$

crystals and an effective separation of the photogenerated charge carriers due to tungsten

doping.[8,18,34] However, with the maximum amount of tungsten dopant ($x = 0.10$), the O_2 evolution

rate abruptly decreased to 31 $\mu mol \cdot h^{-1}$. This decrease can be related to the presence of a large

amount of defect states, which were generated due to the superfluous tungsten doping in the

forbidden band of $LaTiO_2N$.[18,19] Those defect states would likely act as the recombination centers

for the photogenerated electrons and holes.[18,19] The O_2 evolution rate was slightly decreased with

increasing the reaction time because of the deposition of metallic silver nanoparticles on the

surfaces of the flux-grown photocatalyst crystals, and the metallic silver nanoparticles hinder light

absorption and cover surface active sites.[19] With an increase in the amount of tungsten dopant from

$x = 0.00$ to $x = 0.10$, the specific surface areas of the flux-grown crystals decreased in the following

order: 9.5 ($x = 0.00$), 7.7 ($x = 0.01$), 7.3 ($x = 0.02$), 7.1 ($x = 0.05$), and 6.1 ($x = 0.10$) $m^2 \cdot g^{-1}$. With

the maximum amount of tungsten dopant ($x = 0.10$), the lower specific surface area may

additionally contribute to the lowered photocatalytic activity for O_2 evolution.[42] Due to the

14

photodecomposition of the flux-grown oxynitride crystals, a negligible amount of N_2 gas (< 12

μmol) was evolved after 2 h of photocatalytic reaction.[19] The N_2 evolution rate was drastically

diminished with the progress of photocatalytic reaction, indicating the stability of the flux-grown

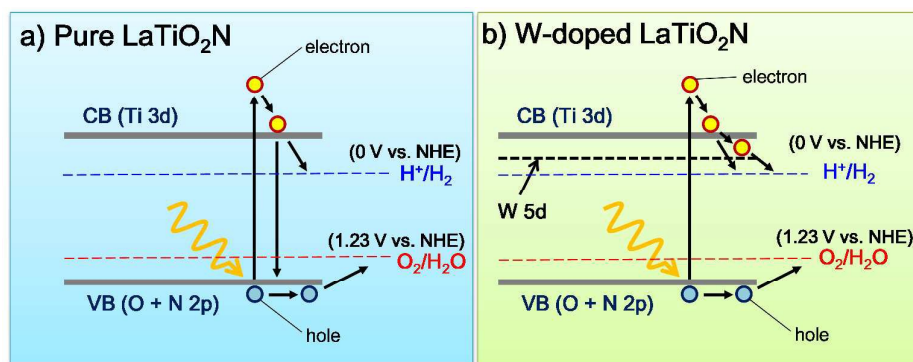oxynitride crystals under the current experimental conditions.

Figure 5. Schematic representation of photocatalytic O_2 evolution over (a) pure $LaTiO_2N$ and (b)

W-doped $LaTiO_2N$ crystals directly grown by an NH_3-assisted KCl flux method.

On the basis of the results obtained in this study and previous reports,[41,43,44] the schematic diagrams

of the $AgNO_3$-assisted O_2 evolution over pure and W-doped $LaTiO_2N$ crystals under visible light

irradiation at pH = 7 is shown in Figure 5. Generally, the W 5d orbital of WO_3 is more positive

potential as compared to the reduction potential of H_2O to generate H_2.[43] Presumably, the W 5d

orbital existing in the W-doped $LaTiO_2N$ crystals can hybridize with Ti 3d orbital and lower the

bottom of conduction band, as shown in Figure 5b. The tungsten dopant and interstitial nitrogen

species are expected to significantly contribute to the change in band gap energy of the W-doped

$LaTiO_2N$. However, according to the previous theoretical calculations, the incorporation of tungsten

in the titanium site led to the shift of Fermi level into the conduction band due to the strong

hybridization of Ti 3d states with W 5d states, causing the broadening of the band gap energy of

W-doped TiO_2.[44] Based on this phenomenon, it is possible that the W-doped $LaTiO_2N$ can act as a

degenerate semiconductor. Moreover, the isolated N 2p narrow band, which consists of interstitial

nitrogen and is located just above the O 2p + N 2p valence band, can additionally contribute to the

improvement of photocatalytic water oxidation activity of the W-doped $LaTiO_2N$ because of the

enhanced light absorption and narrowed band gap.[41]

Figure 6 shows the local densities of states (LDOS) for (a) LTON, (b) W-LTON, and (c) LTO

calculated by HSE06 functional, and the estimated band gaps are 2.3, 2.3, and 3.4 eV, respectively.

The calculated band gaps for LTON and W-LTON (about 2.3 eV) are in accordance with the band

gaps experimentally obtained in this study (2.03 – 2.11 eV). Note that the conventional GGA

functional is prone to underestimate the band gap, indicating about 1.3 eV for LTON in the present

calculation (not shown here). Therefore, the calculated electronic structure based on the HSE06

calculations is discussed hereinafter unless specially mentioned. Obviously, the band gap of pure

oxide (LTO) is much larger than that of oxynitrides (LTON, W-LTON). In detail, the top of valence

band of LTO is mainly formed by O 2p orbital, whereas N 2p orbital is visible at the top of valence

band followed by O 2p orbital at lower energy level in oxynitrides. A significant decrease in band

gap achieved by introducing the nitride ions into the LTO framework is primarily due to the

elevation of the top of valence band by N 2p orbital.[45] Figure 7a shows the partial electron density

for the top of valence band (ranging from -1 eV to 0 eV in Figure 6b) for W-LTON, and the partial

16

electron densities are mainly distributed around the nitride ions. The bottom of conduction band is

mainly composed of Ti 3d orbital for the three models of LTON, W-LTON, and LTO. Note that W

5d and 6s orbitals are also located at the bottom of conduction band, but no significant change in

band gap is indicated. The partial electron density distribution at the bottom of conduction band

(ranging from 2.3 eV to 3 eV in Figure 6b for W-LTON also indicates that the conduction band is

mainly composed of both Ti and W t_{2g} orbitals, as shown in Figure 7b. Although no significant

change in band gap by W doping was observed, a slight broadening of valence and conduction

bands was noted in W-LTON which may improve the electron/hole conductivity due to reducing
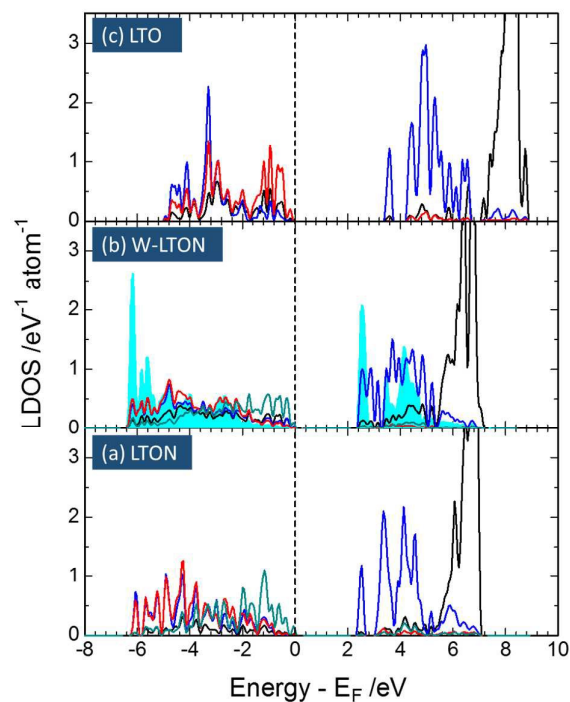
the effective mass of electron.

Figure 6. Local density of states (LDOS) for (a) LaTiO$_2$N (LTON), (b) W-doped LTON

(W-LTON), and (c) [LaTiO$_3$]$^+$ (LTO) obtained by first-principles calculations using HSE06 hybrid

17

functional. Black, dark blue, red, green, and light blue lines represent the LDOS of La, Ti, O, N, and W, respectively. The energy scale is aligned so that the Fermi level is to be zero.
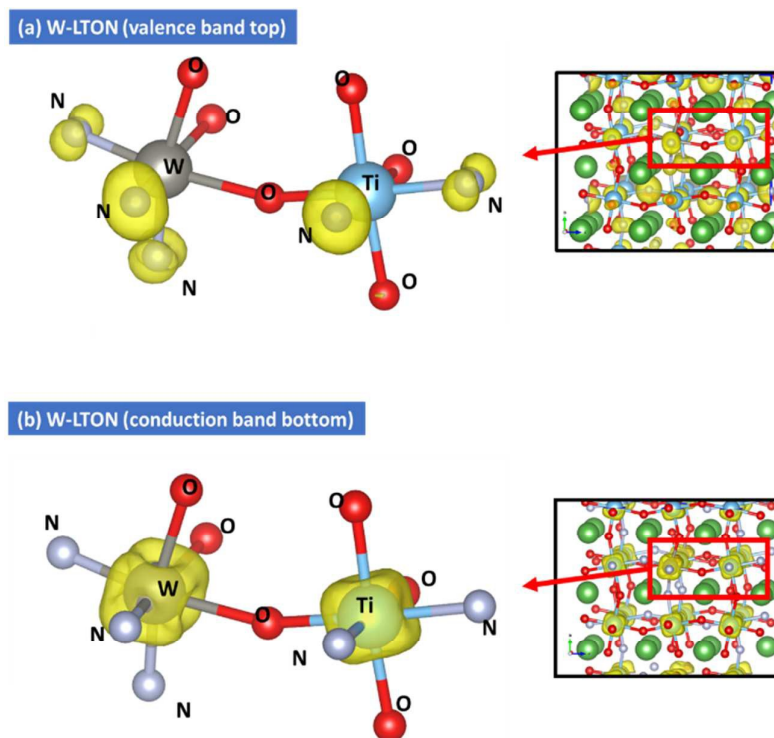

Figure 7. Calculated partial electron density distribution for W-doped $LaTiO_2N$ (W-LTON). Panels (a) and (b) represent the partial electron density at the top of valence band (from -1 to 2 eV in Figure 6b) and the bottom of conduction band (from 2.3 to 3 eV), respectively. The isosurface level is set to be 0.02 $Å^{-3}$. In panel (a), N 2p orbital is clearly visible due to its dumbbell shape orbital. In panel (b), the orbital is not directed to the ligands (oxide or nitride ion), indicating that the bottom of conduction band, both at W and Ti sites, is mainly composed of t_{2g} type orbital.

Conclusions

To conclude, $LaTi_{1-x}W_x(O,N)_3$ (x = 0.00 - 0.10) crystals were directly grown by an NH_3-assisted flux method using the KCl flux. With the maximum amount of tungsten dopant (x = 0.10), $LaWO_{0.6}N_{2.4}$ was formed as an impurity phase to the W-doped $LaTiO_2N$ phase. The W-doped $LaTiO_2N$ crystals grown with x = 0.00 – 0.05 in a rounded shape had average sizes of *ca.* 178, 234, 227, and 206 nm, respectively, whereas the crystals grown with x = 0.10 possessed two different morphologies: small rounded (*ca.* 210 nm in size) and large cuboid (*ca.* 396 nm in size). An increase in the amount of tungsten dopant resulted in a slight decrease in the specific surface area from 9.5 to 6.1 $m^2 \cdot g^{-1}$. From the first-principles density function theory (DFT) calculations, a slight broadening of valence and conduction bands was observed in W-LTON which may improve the electron/hole conductivity due to reducing the effective mass of electron. Considering the first 2 h of the photocatalytic water oxidation reaction, the W-doped $LaTiO_2N$ crystals grown with x = 0.05 showed higher O_2 evolution rate (51 $\mu mol \cdot h^{-1}$) compared with pure $LaTiO_2N$ crystals (18 $\mu mol \cdot h^{-1}$) due to the improved conductivity, enhanced light absorption, and efficient charge separation.

Acknowledgements

References

1 K. Maeda and K. Domen, *J. Phys. Chem. C*, 2007, **111**, 7851–7861.

2 S. G. Ebbinghaus, H.-P. Abicht, R. Dronskowski, T. Müller, A. Reller and A. Weidenkaff, *Prog. Solid State Chem.*, 2009, **37**, 173–205.

3 A. Kasahara, K. Nukumizu, G. Hitoki, T. Takata, J. N. Kondo, M. Hara, H. Kobayashi and K. Domen, *J. Phys. Chem. A*, 2002, **106**, 6750–6753.

4 A. Kasahara, K. Nukumizu, T. Takata, J. N. Kondo, M. Hara, H. Kobayashi and K. Domen, *J. Phys. Chem. B*, 2003, **107**, 791–797.

5 K. Maeda, *Phys. Chem. Chem. Phys.*, 2013, **15**, 10537–10548.

6 W. Luo, Z. Li, X. Jiang, T. Yu, L. Liu, X. Chen, J. Ye and Z. Zou, *Phys. Chem. Chem. Phys.*, 2008, **10**, 6717–6723.

7 A. E. Maegli, T. Hisatomi, E. H. Otal, S. Yoon, S. Pokrant, M. Grätzel and A. Weidenkaff, *J. Mater. Chem.*, 2012, **22**, 17906–17913.

8 A. E. Maegli, L. Sagarna, S. Populoh, B. Penkala, E. H. Otal and A. Weidenkaff, *J. Solid State Chem.*, 2014, **211**, 106–112.

9 C. M. Leroy, A. E. Maegli, K. Sivula, T. Hisatomi, N. Xanthopoulos, E. H. Otal, S. Yoon, A. Weidenkaff, R. Sanjines and M. Grätzel, *Chem. Commun.*, 2012, **48**, 820–822.

10 F. Zhang, A. Yamakata, K. Maeda, Y. Moriya, T. Takata, J. Kubota, K. Teshima, S. Oishi and K. Domen, *J. Am. Chem. Soc.*, 2012, **134**, 8348–8351.

11 J. Feng, W. Luo, T. Fang, H. Lv, Z. Wang, J. Gao, W. Liu, T. Yu, Z. Li and Z. Zou, *Adv. Func. Mater.* 2014, **24**, 3535–3542.

12 M. Hojamberdiev, A. Yamaguchi, K. Yubuta, S. Oishi and K. Teshima, *Inorg. Chem.*, 2015, **54**, 3237–3244.

13 K. Kawashima, M. Hojamberdiev, H. Wagata, K. Yubuta, S. Oishi and K. Teshima, *Cryst. Growth Des.*, 2015, **15**, 333–339.

14 A. E. Maegli, S. Pokrant, T. Hisatomi, M. Trottmann, K. Domen and A. Weidenkaff, *J. Phys. Chem. C*, 2014, **118**, 16344–16346.

15 K. Kawashima, M. Hojamberdiev, H. Wagata, K. Yubuta, J. J. M. Vequizo, A. Yamakata, S. Oishi, K. Domen and K. Teshima, *J. Phys. Chem. C*, 2015, **119**, 15896–15904.

16 X. Zhang, F. Liu, Q.-L. Huang, G. Zhou and Z.-S. Wang, *J. Phys. Chem. C*, 2011, **115**, 12665–12671.

17 L. Chen, F. M. Toma, J. K. Cooper, A. Lyon, Y. Lin, I. D. Sharp and J. W. Ager, *ChemSusChem*, 2015, **8**, 1066–1071.

18 S. Grigorescu, B. Bärhausen, L. Wang, A. Mazare, J. E. Yoo, R. Hahn and P. Schmuki, *Electrochem. Commun.*, 2015, **51**, 85–88.

19 K. Maeda, D. Lu and K. Domen, *Angew. Chem. Int. Ed.*, 2013, **52**, 6488–6491.

20 G. Kresse and J. Furthmüller, *Compt. Mater. Sci.*, 1996, **6**, 15–50.

21 G. Kresse and J. Furthmüller, *Phys. Rev. B*, 1996, **54**, 11169.

22 J. P. Perdew, K. Burke and M. Ernzerhof, *Phys. Rev. Lett.*, 1996, **77**, 3865.

23 J. P. Perdew, A. Ruzsinszky, G. I. Csonka, O. A. Vydrov, G. E. Scuseria, L. A. Constantin, X. Zhou and K. Burke, *Phys. Rev. Lett.*, 2008, **100**, 136406.

24 P. E. Blöchl, *Phys. Rev. B*, 1994, **50**, 17953.

25 M. Yashima, M. Saito, H. Nakano, T. Takata, K. Ogisu and K. Domen, *Chem. Commun.*, 2010, **46**, 4704–4706.

26 J. L. F. Da Silva, M. V. Ganduglia-Pirovano, J. Sauer, V. Bayer and G. Kresse, *Phys. Rev. B*, 2007, **75**, 045121.

27 V. L. Chevrier, S. P. Ong, R. Armiento, M. K. Y. Chan and G. Ceder, *Phys. Rev. B*, 2010, **82**, 075122.

28 M. K. Aydinol, A. F. Kohan, G. Ceder, K. Cho and J. Joannopoulos, *Phys. Rev. B*, 1997, **56**, 1354.

29 Y. Q. Jia, *J. Solid State Chem.*, 1991, **95**, 184–187.

30 Y. Wu, X. Hu, T. Xie, G. Li and L. Zhang, *China Partic.*, 2005, **3**, 233–236.

31 T. Nathan-Walleser and L. J. Xiang, *Int. J. Mater. Sci.* 2013, **3**, 104–109.

32 H. Tian, J. Ma, K. Li and J. Li, *Mater. Chem. Phys.*, 2008, **112**, 47–51.

33 M. Zhang, J. Wu, D. Lu and J. Yang, *Int. J. Photoenergy*, 2013, **2013**, 471674.

34 J. Li, J. Xu, W. L. Dai, H. Li and K. Fan, *Appl. Catal. B*, 2008, **82**, 233–243.

35 M. Perez, *Scripta Mater.*, 2005, **52**, 709‑712.

36 P. Bacher, P. Antoine, R. Marchand, P. L'Haridon, Y. Laurent and G. Roult, *J. Solid State Chem.*, 1988, **77**, 67–71.

37 M. Hojamberdiev, K. Yubuta, J. J. M. Vequizo, A. Yamakata, S. Oishi, K. Domen and K. Teshima, *Cryst. Growth Des*, 2015, **15**, 4663–4671.

38 K. A. Michalow, A. Vital, A. Heel, T. Graule, F. A. Reifler, A. Ritter, K. Zakrzewska, and M. Rekas, *J. Adv. Oxid. Technol.*, 2008, **11**, 56–64.

39 C. Hua, X. Dong, X. Wang, M. Xue, X. Zhang and H. Ma, *J. Nanomater.*, 2014, **2014**, 943796.

40 M. Yashima, M. Saito, H. Nakano, T. Takata, K. Ogisu and K. Domen, *Chem. Commun.*, 2010, **46**, 4704–4706.

41 F. Peng, L. Cai, H. Yu, H. Wang and J. Yang, *J. Solid State Chem.*, 2008, **181**, 130–136.

42 S. Landsmann, A. E. Maegli, M. Trottmann, C. Battaglia, A. Weidenkaff and S. Pokrant, *ChemSusChem*, 2015, **8**, 3451–3458.

43 S. Ikeda, T. Itani, K. Nango and M. Matsumura, *Catal. Lett.*, 2004, **98**, 229–233.

44 D. Chen, G. Xu, L. Miao, L. Chen, S. Nakao and P. Jin, *J. Appl. Phys.*, 2010, **107**, 063707.

45 M. Hojamberdiev, H. Wagata, K. Yubuta, K. Kawashima, J. J. M. Vequizo, A. Yamakata, S. Oishi, K. Domen and K. Teshima, *Appl. Catal. B*, 2016, **182**, 626–635.

For Table of Contents Only
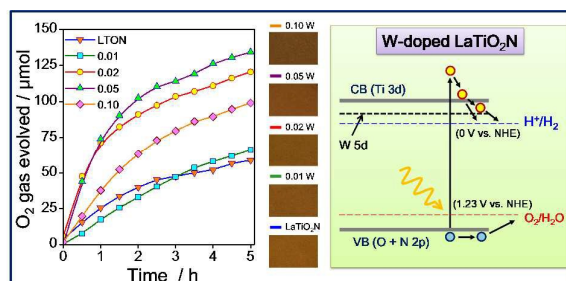
Effect of tungsten dopant on photocatalytic water oxidation activity of $LaTiO_2N$ crystals grown by an NH_3-assisted flux method was studied.